3D Segmentation of Prostate Ultrasound images Using Wavelet Transform

Hamed Akbari, **Xiaofeng Yang**, **Luma V. Halig**, and **Baowei Fei**[*]
Department of Radiology, Emory University, 1841 Clifton Rd, NE, Atlanta, GA, USA 30329

Abstract

The current definitive diagnosis of prostate cancer is transrectal ultrasound (TRUS) guided biopsy. However, the current procedure is limited by using 2D biopsy tools to target 3D biopsy locations. This paper presents a new method for automatic segmentation of the prostate in three-dimensional transrectal ultrasound images, by extracting texture features and by statistically matching geometrical shape of the prostate. A set of Wavelet-based support vector machines (W-SVMs) are located and trained at different regions of the prostate surface. The WSVMs capture texture priors of ultrasound images for classification of the prostate and non-prostate tissues in different zones around the prostate boundary. In the segmentation procedure, these W-SVMs are trained in three sagittal, coronal, and transverse planes. The pre-trained W-SVMs are employed to tentatively label each voxel around the surface of the model as a prostate or non-prostate voxel by the texture matching. The labeled voxels in three planes after post-processing is overlaid on a prostate probability model. The probability prostate model is created using 10 segmented prostate data. Consequently, each voxel has four labels: sagittal, coronal, and transverse planes and one probability label. By defining a weight function for each labeling in each region, each voxel is labeled as a prostate or non-prostate voxel. Experimental results by using real patient data show the good performance of the proposed model in segmenting the prostate from ultrasound images.

Keywords

Prostate segmentation; Ultrasound image segmentation; Wavelet based segmentation; Support Vector Machines; kernel support vector machine; transrectal ultrasound image

1. INTRODUCTION

Segmentation of different organs and tissues in ultrasound images is one of the most challenging tasks in medical image processing. Ultrasound image segmentation has been studied by many researchers to automatically detect or track the anatomical structures during image-guided medical procedures. Prostate segmentation is one of the most important and practical applications of ultrasound image segmentation. Segmentation of three-dimensional (3-D) transrectal ultrasound (TRUS) images may be utilized in prostate cancer biopsy and image-guided surgical planning and therapy [1]. Comparing to magnetic resonance imaging (MRI) or computed tomography (CT), US is inexpensive and easy to use and is able to follow deformation in real time. A reliable and accurate method to detect the prostate boundaries would be useful during many procedures on the prostate such as inserting a needle for biopsy [2], planning for brachytherapy [3], and the volume measurement of the prostate gland. So far, automatic prostate segmentation has remained as a problematic issue

in TRUS. It is often required manual segmentation of the prostate. However, this segmentation is time consuming. Many methods for semi-automatic or automatic segmentation of the prostate in TRUS images have been proposed. Knoll et al. proposed a deformable segmentation model that uses one-dimensional wavelet transform as a multi-scale contour parameterization tool to constrain the shape of the prostate model [4]. Pathak et al. developed a model for an edge-guided definition that provides the detected prostate edges as a visual guidance for the user to manually edit the boundaries [5]. Richard et al. used a texture-based method that employs a clustering process to label the prostate region based on four-texture energy [6]. Ghanei et al. designed a 3-D discrete model to outline the prostate boundaries [7]. A user is required to outline the prostate in several two-dimensional (2-D) cross-sections of the volume image in order to provide an initialization model. Zhan and Shen proposed a 3-D shape model for automatically segmenting 3-D prostate boundary from 3-D TRUS images using shape statistics and Gabor features [1].

Hu et al. presented a semi-automatic approach that used a model-based initialization and mesh refinement that initialized by only six manually selected points on the prostate boundary [8]. Active shape models (ASM) was proposed to segment the prostate [9] as well as other organs [10]. Level set framework was also applied to segment the prostate [11] and other tissue [12]. Atlas registration and statistical texture prior was utilized to automatically segment the TRUS [13]. In this paper, we propose a 3-D model for automatically segmenting 3-D prostate in 3-D TRUS images using Wavelet features and prostate geometry.

2. METHODS

The proposed method consists of the training and application stages. Two training TRUS images were used for wavelet features training and ten patients are used to make a predefined model. The prostate boundaries have been manually defined by specialists. A prostate shape model is created based on the allowable models of shape variations and its probability. This model is employed to modify the prostate boundaries. The prostate textures are locally captured by training the locally placed Wavelet-based support vector machines (W-SVMs). With integrating local texture features and geometrical data, W-SVMs can robustly differentiate the prostate tissue from the adjacent tissues. The trained W-SVMs are employed to tentatively label the respective voxels around the surface into prostate and non-prostate tissues based on their texture features from different Wavelet filters. Subsequently, after an affine transformation of the shape model to the pre-defined prostate region that optimally matches with the texture features of the prostate boundary, the surface of the model is driven to the boundary between the tentatively labeled prostate and non-prostate tissues based on defined weighting functions and labeled voxels.

2.1 W-SVMs

US image textures can provide important features for accurately defining the prostate, especially for the regions where prostate boundaries are not clear. Biorthogonal wavelets 1.3, 1.5, and 4.4 are employed to extract the texture features of the prostate. Designing biorthogonal wavelets allows more degrees of freedom comparing to orthogonal wavelets. One additional degree of freedom is the possibility to construct symmetric wavelet functions. A number of W-SVMs on different regions of the surface model are placed and trained to adaptively label the tissue based on its texture and location. Each W-SVM is composed of 5 wavelet filter banks, voxel coordinates, and a Kernel Support Vector Machine (KSVM). Figure 1 shows wavelet filters that were employed for feature extraction.

The wavelet filters are employed to extract texture features from TRUS images, and the KSVM is used to nonlinearly classify the Wavelet texture features for tissue differentiation.

Each W-SVM corresponds to an individual sub-region in order to characterize and differentiate image textures locally and adaptively. All W-SVMs are trained to differentiate the texture features around its corresponding sub-regions in the training set. The trained W-SVMs are employed to tentatively label each voxel into prostate and non-prostate tissues in the application stage. To find more accurate segmentation, the set of W-SVMs is trained and applied in 3 planes (sagittal, coronal, transverse). Three sets of 2-D Wavelet filters were located at three orthogonal planes and were trained in each plane. Therefore, each voxel was tentatively labeled in three planes as prostate or non-prostate voxel. Figure 2 shows the algorithm flowchart of the segmentation method.

2.2 Probability model

A prostate probability model was used for modifying the segmentation. Previously, we proposed several methods for prostate registration [14–16]. In this study, we registered ten segmented prostates using an affine transformation. The registration approach that employed for creating the model is based on the principal axis transformation. This method was chosen because of its computational properties, speed and simplicity. The prostate volume was translated and rotated with respect to each other. The principal axis transformation is known from the classical theory of rigid bodies. A rigid body is uniquely located by knowledge of the position of its center of mass and its orientation (rotation) with respect to its center of mass. The center of mass, inertia matrix, and principal axes can be determined for any rigid body. For simple geometric shapes, the principal axes coincide with the axes of symmetry. In general, an orthogonal coordinate system is set up with their origin at the center of mass. When computed in the principal axis coordinate system, the inertia matrix is diagonal [17]. The basic parameters that were used for registration of the prostate are the position of the center of mass and rotation of the prostate about the center of mass, and the lengths of the principle axes. These properties uniquely determine the location and geometry of the prostate in three-dimensional space. After overlaying these 10 registered volumes, a probability model was created for each voxel based on how many prostate models are labeled as a voxel of the prostate at that region. Figure 3 shows a few 2-D segmentation results in different planes.

2.3 Evaluation Criteria

We validate the segmentation using Dice similarity ratio and sensitivity [18–19]. Quantitative performance assessment of the method was performed by comparing the results with the gold standard data. The Dice similarity was used to numerically assess the prostate classification algorithm. The Dice similarity was computed as follows:

$$Dice(S,G) = \frac{2|S \cap G|}{|S|+|G|} \times 100\%, \tag{1}$$

where S represents the voxel set of the prostate segmentation results obtained by the algorithm and G represents the voxel set of the corresponding gold standard data.

Sensitivity, $Sen(S,G)$, represents the proportion of the segmented prostate volume, S, that is correctly overlapped with the gold standard volume, G.

$$Sen(S,G) = TP/G \times 100\%, \tag{2}$$

where TP is the true positive volume and represents the overlapped volume of the segmented prostate and the gold standard. When a voxel was not detected as a prostate voxel, the detection was considered false negative if the voxel was indeed a voxel of the prostate on the gold standard that was established by manual segmentation. When a voxel

was detected as a prostate voxel, the detection was a false positive if the voxel was not a prostate voxel on the gold standard.

3. RESULTS

The method was evaluated by five patient data sets of 3-D TRUS. Fig. 3 shows sample segmentation and its comparison with the corresponding gold standard. Quantitative performance assessment of the method was done by comparing the results with the corresponding gold standard data from manual segmentation. The Dice similarity and Sensitivity were used as performance assessment metrics in prostate classification algorithm. The numerical results of these evaluation criteria are shown in Table 1. The dice ratio is between 88.7%–95.0% among five prostate volumes. The mean and standard deviation of the dice function are 90.7% and 2.5% respectively.

4. DISCUSSION AND CONCLUSION

A set of Wavelet-based support vector machines (W-SVMs) and a shape model are developed and evaluated for automatic segmentation of the prostate TRUS images. Wavelet transform was employed for prostate texture extraction. A probability prostate model was incorporated into the approach to improve the robustness of the segmentation. This paper has presented a new method for segmenting the prostate from 3-D TRUS images, using both the prostate shape and texture features. A set of W-SVMs are located at different regions of the surface to classify prostate and non-prostate tissues in different zones around the prostate boundary. Compared to 2-D prostate segmentation methods, the proposed method can segment the prostate in three dimensions. This method employs a learning based mechanism, using W-SVMs, to automatically collect texture features in different regions of prostate boundary. The probability model was incorporated into the segmented model to locally and adaptively identify prostate and non-prostate tissues. In this way, even if the prostate has diverse appearance in different parts and weak boundary near bladder or rectum, the model is still able to produce a relatively accurate segmentation in 3-D TRUS images.

Acknowledgments

References

1. Zhan Y, Shen D. Deformable segmentation of 3-D ultrasound prostate images using statistical texture matching method. IEEE Trans Med Imaging. 2006; 25(3):256–273. [PubMed: 16524083]

2. Hodge KK, McNeal JE, Terris MK, Stamey TA. Random-systematic versus directed ultrasound-guided core-biopsies of the prostate. J Urol. 1989; 142:71–75. [PubMed: 2659827]

3. Grimm PD, Balsko JC, Ragde H. Ultrasound guided transperineal implantation of iodine 125 and palladium 103 for the treatment of early stage prostate cancer. Atlas Urol Clin No Amer. 1994; 2:113–125.

4. Knoll C, Alcaniz M, Grau V, Monserrat C, Juan MC. Outlining of the prostate using snakes with shape restrictions based on the wavelet transform. Pattern Recognit. 1999; 32:1767–1781.

5. Pathak SD, Chalana V, Haynor DR, Kim Y. Edge-guided boundary delineation in prostate ultrasound images. IEEE Trans Med Imag. 2000; 19(12):1211–1219.

6. Richard WD, Keen CG. Automated texture-based segmentation of ultrasound images of the prostate. Computerized Medical Imaging and Graphics. 1996; 20:131–140. [PubMed: 8930465]

7. Ghanei A, Soltanian-Zadeh H, Ratkesicz A, Yin F. A three-dimensional deformable model for segmentation of human prostate from ultrasound image. Med Phys. 2001; 28:2147–2153. [PubMed: 11695777]

8. Hu N, Downey DB, Fenster A, Ladak HM. Prostate boundary segmentation from 3D ultrasound images. Medical Physics. 2003; 30:1648–1659. [PubMed: 12906182]

9. Hodge AC, Fenster A, Downey DB, Ladak HM. Prostate boundary segmentation from ultrasound images using 2D active shape models: Optimisation and extension to 3D. Computer Methods and Programs in Biomedicine. 2006; 84:99–113. [PubMed: 16930764]

10. Guo S, Fei B. A minimal path searching approach for active shape model (ASM)-based segmentation of the lung. Proc SPIE. 2009; 7259:72594B.

11. Yang F, Suri J, Fenster A. Segmentation of prostate from 3-D ultrasound volumes using shape and intensity priors in level set framework. Conf Proc IEEE Eng Med Biol Soc. 2006; 1:2341–4. [PubMed: 17945709]

12. Zhang H, Bian Z, Guo Y, Fei B, Ye M. An efficient multiscale approach to level set evolution. Conf 25th Proc IEEE Eng Med Biol Soc. 2003; 1:694–697.

13. Yang X, Schuster D, Master V, Nieh P, Fenster A, Fei B. Automatic 3D Segmentation of Ultrasound Images Using Atlas Registration and Statistical Texture Prior. Proc SPIE. 2011:7964.

14. Fei B, Duerk JL, Sodee DB, Wilson DL. Semiautomatic nonrigid registration for the prostate and pelvic MR volumes. Academic Radiology. 2005; 12:815–24. [PubMed: 16039535]

15. Fei B, Lee Z, Duerk JL, Lewin JS, Sodee DB, Wilson DL. Registration and Fusion of SPECT, High Resolution MRI, and interventional MRI for Thermal Ablation of the Prostate Cancer. IEEE Transactions on Nuclear Science. 2004; 51(1):177–183.

16. Yang X, Akbari H, Halig L, Fei B. 3D non-rigid registration using surface and local salient features for transrectal ultrasound image-guided prostate biopsy. Proc SPIE. 2011:7964.

17. Alpert NM, Bradshaw JF, Kennedy D, Correia JA. The principal axes transformation a method for image registration. The Journal of Nuclear Medicine. 1990; 31(10):1717–1722.

18. Wang H, Fei B. A modified fuzzy C-means classification method using a multiscale diffusion filtering scheme. Med Image Anal. 2009; 13(2):193–202. [PubMed: 18684658]

19. Cool D, Downey D, Izawa J, Chin J, Fenster A. 3D prostate model formation from non-parallel 2D ultrasound biopsy images. Medical Image Analysis. 2006; 10:875–887. [PubMed: 17097333]
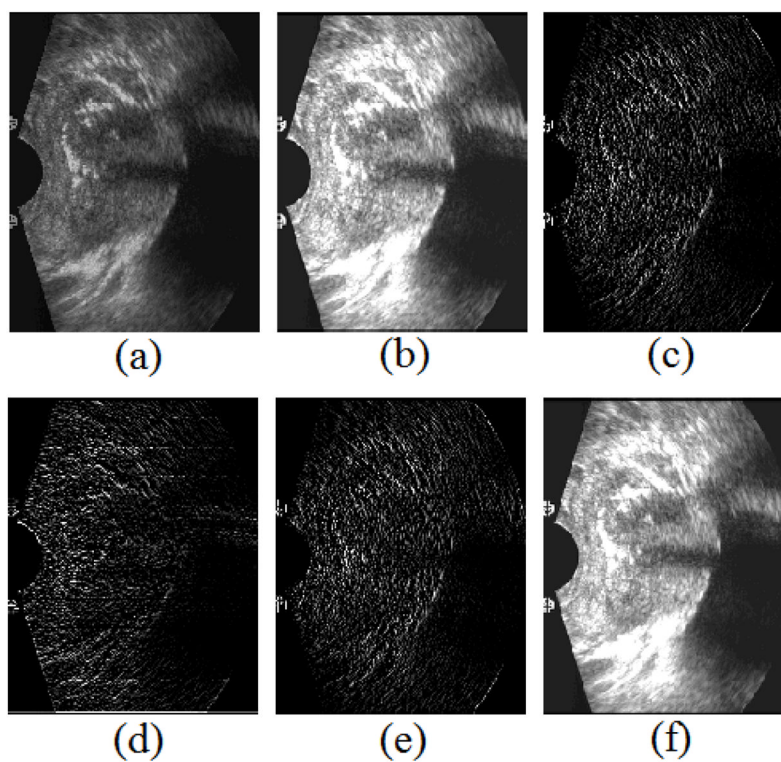
Figure 1.
Wavelet filters that were employed for feature extraction: (a) Original image, (b) Biorthogonal 1.3 first approximation, (c) Biorthogonal 1.3 vertical details, (d) Biorthogonal 1.5 horizontal details, (e) Biorthogonal 1.5 vertical details, (f) Biorthogonal 4.4 first approximation.
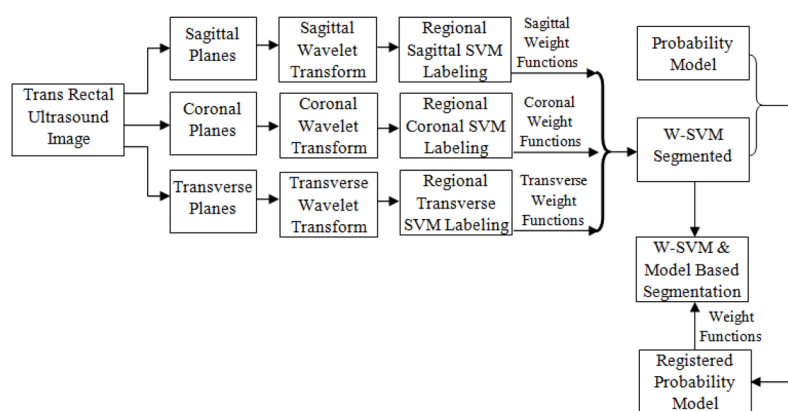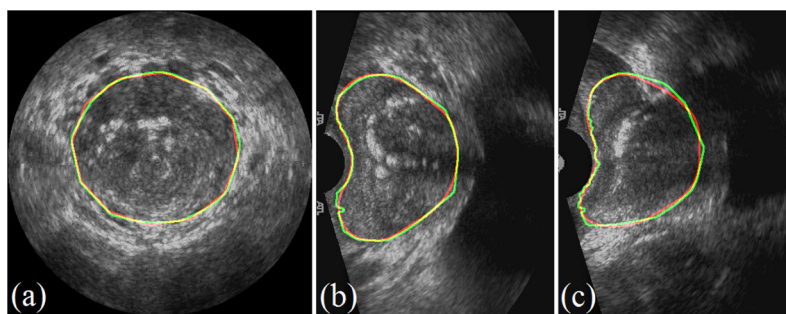
Figure 2.
The algorithm flowchart.

Figure 3.
2-D segmentation results in different planes: red lines are the gold standard boundaries and green lines are the segmentation boundaries. (a) Coronal plane (b) Sagittal plane (c) Transverse plane.
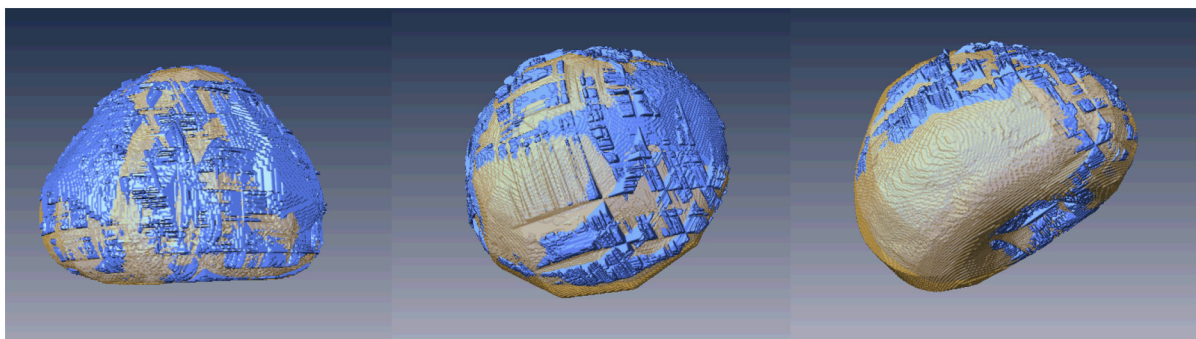
Figure 4.
Different views of a 3-D result of the prostate segmentation (shown in blue) and its comparison with the corresponding gold standard (shown in gold, transparent).

Table 1

Quantitative evaluation results.

	Patient 1	Patient 2	patient 3	patient 4	Patient 5	Mean	Standard Deviation
DICE	90.2%	88.7%	88.9%	95.0%	90.8%	90.7%	2.5%
Sensitivity	91.2%	95.2%	82.3%	93.6%	91.1%	90.7%	4.9%